Model for noncollisional heating in inductively coupled plasma processing sources

Shahid Rauf[a] and Mark J. Kushner[b]
Department of Electrical and Computer Engineering, University of Illinois, 1406 West Green Street, Urbana, Illinois 61801

(Received 9 December 1996; accepted for publication 20 January 1997)

Low pressure (<10 mTorr) inductively coupled plasma sources are being developed for etching and deposition of semiconductors and metals. In models for these devices, plasma dynamics are typically coupled to the electromagnetic fields through Ohm's law, which implies that collisional heating is the dominant power transfer mechanism. In this article, we describe an algorithm to couple plasma dynamics to electromagnetic field propagation which self-consistently includes noncollisional heating effects as well. The algorithm makes use of kinetic information available from an electron Monte Carlo simulation to compute plasma currents that are then used in computation of the electromagnetic field. Results for plasma density and electric field amplitude are presented as a function of power and pressure, and are compared to results from models that consider only collisional heating. We find that noncollisional heating effects are important at pressures of less than 10–20 mTorr, a range that depends both on gas mixture and geometry. Noncollisional heating effects allow the wave to couple more efficiently to the plasma. As a result, the electric field amplitude required to deposit a given amount of power in the plasma is smaller than that needed when only collisional heating is considered. For a constant power deposition, this generally leads to lower plasma densities. [S0021-8979(97)03609-8]

I. INTRODUCTION

Plasmas are extensively used in the microelectronics fabrication industry for etching and deposition of semiconductor materials and metals. Among the new tools that are being developed for these applications, inductively coupled plasma (ICP) reactors have attracted considerable attention. As compared to conventional capacitively coupled reactive ion etching (RIE) discharges, ICP reactors operate at higher plasma densities (10^{11}–10^{12} cm^{-3}) and lower gas pressures (1–20 mTorr). These reactors typically have separate power supplies for the radio frequency (rf) antenna and substrate bias. This configuration has the advantage that the magnitude and energy of the wafer-directed ion flux can be separately controlled. The bias, and hence voltage drop across the sheaths, is also typically smaller in ICP reactors than in RIE discharges. This reduces the energy with which the ions bombard the wafer surface and hence minimizes wafer damage. Although ICPs have been in use for a number of years, it was only recently that they were widely adopted for semiconductor processing applications. The first designs were described in patents by Coultas and Keller[1] and Ogle.[2] The reactors used in later experiments by Wendt *et al.*,[3,4] Hopwood *et al.*,[5–8] Godyak *et al.*,[9,10] and Hebner *et al.*[11,12] operate on a similar principle. Several groups have also developed detailed numerical models of these reactors with the goal of yielding insight to the underlying physical processes as well as proposing methods to improve plasma uniformity and reactor performance.[13–16]

In ICP reactors, the plasma is created and sustained by the electromagnetic wave that is generated by an external rf antenna. Since all plasma parameters depend sensitively on the magnitude and profile of the wave electromagnetic fields, it is important to properly represent the coupling of the plasma and electromagnetic wave in models of ICP reactors. Traditionally, the plasma dynamics in models of low pressure plasmas are coupled back to the electromagnetic fields under the assumption of a collision-dominated cold plasma. In this situation, one can define an effective conductivity for the plasma, and relate the plasma current to the electric field using Ohm's law. This formulation contains the implicit assumption that the only manner in which the electromagnetic field transfers random thermal energy to the plasma is through collisional heating. It was shown by Turner,[17] however, that other noncollisional heating mechanisms might compete or even overshadow collisional heating in the parameter regime (pressure and characteristic dimensions) in which ICP reactors are generally operated. Turner attributed these noncollisional heating mechanisms to warm plasma effects. Godyak, Piejak, and Alexandrovich[18] observed evidence of noncollisional heating during electrical measurements in ICP reactors. They speculated that the underlying mechanism is analogous to the anomalous skin effect in superconductors.

Noncollisional heating effects were first included in a large-scale ICP simulation by Vahedi *et al.*[19] Their approach was to define an effective collision frequency that would take into account noncollisional heating. The physical process that was used to derive the effective conductivity was similar to that for stochastic heating in capacitive discharges. These studies[17–19] indicate that a number of distinguishable heating mechanisms can be present in the plasma.

[a]Electronic mail: rauf@uigela.ece.uiuc.edu
[b]Electronic mail: mjk@uiuc.edu

 0021-8979/97/81(9)/5966/9/$10.00

We have developed a methodology to directly couple plasma dynamics to the electromagnetic field computation in models of ICPs and implemented the algorithm in a hybrid computational model for ICP reactors. In this model, the electron kinetics are addressed by a Monte Carlo simulation while the electromagnetic fields are computed by solving Maxwell's equations in a separate module. Our technique allows us to evaluate the multidimensional dynamics resulting from acceleration of electrons in the presence of sparse collisions in the Monte Carlo simulation, and feed that information back to the electromagnetics calculations. In principle, the resulting model should be valid no matter which heating mechanisms dominate in a given situation. In this article, we describe this technique, and discuss its implications on the computed steady-state plasma parameters and electromagnetic wave characteristics of ICP reactors as used in materials processing.

In Sec. II, we describe the algorithm and briefly discuss the plasma model. The model was parameterized over a range of gas pressure and power in Ar, O_2, N_2, and Ar/Cl_2 plasmas, and these results are described in Sec. III. Section IV contains our concluding remarks.

II. DESCRIPTION OF THE ALGORITHM AND ITS IMPLEMENTATION

The externally generated electromagnetic waves that produce the plasma in an ICP reactor are described by Maxwell's equations. Assuming that $\nabla \cdot \mathbf{E} = 0$, we find that the electric field $\mathbf{E}$ is governed by

$$\nabla^2 \mathbf{E} + (\omega^2/c^2)\mathbf{E} = i\omega\mu_0 \mathbf{J}, \tag{1}$$

where $\mathbf{J}$, ω, c, and μ_0 are, respectively, the current density, frequency, speed of light, and vacuum permeability. It has been assumed that all wave quantities vary harmonically in time with an $e^{i\omega t}$ dependence. The current density $\mathbf{J}$ contains contributions from the external antenna current as well as the current that is generated in the plasma due to the electromagnetic wave. The plasma exercises its influence on the electromagnetic fields through $\mathbf{J}$. To solve Eq. (1), a number of approximations is generally applied to relate $\mathbf{J}$ and $\mathbf{E}$. The most common among these is the cold-electron approximation, in which the electron momentum conservation equation in the steady state is used to obtain

$$\mathbf{J}_e = \sigma \mathbf{E}, \quad \sigma(\mathbf{r}) = \frac{q^2 n_e(\mathbf{r})}{m_e[\nu_m(\mathbf{r}) + i\omega]}, \tag{2}$$

where $\mathbf{J}_e$, σ, q, m_e, n_e, and ν_m, respectively, designate the electron current density, conductivity, magnitude of electron charge, electron mass, electron density, and electron momentum transfer collision frequency. One typically ignores ion current due to the low ion mobility and uses Eq. (2) to solve for $\mathbf{E}$ from Eq. (1). The collisional power deposition P_c is then

$$P_c = 0.5 \int \sigma_r(\mathbf{r}) E^2(\mathbf{r}) d^3 v, \tag{3}$$

where σ_r is the real component of the conductivity, E is the amplitude of electric field, and the integral is over the volume of the plasma.

The use of the cold-electron approximation has several implications. First, the only mechanism available for conversion of wave energy to random electron thermal energy (i.e., electron heating) is electron collisions with heavy particles. Second, Eq. (2) implies that the current at a particular location in the plasma depends only on the local electromagnetic fields and plasma parameters. If the electron mean free path is sufficiently long that the electron crosses into a region having a different electric field or plasma density, that is, thermal effects are important, the relationship in Eq. (2) is no longer valid. These conditions produce nonlocal effects which cause current at a particular point in the plasma to be influenced by the electric field at other locations as well. In such a situation, the common procedure is to use Boltzmann's equation to define a conductivity tensor $\boldsymbol{\sigma}(\mathbf{r}, \mathbf{r}_1, t, t_1)$. Using $\boldsymbol{\sigma}$, $\mathbf{J}$ and $\mathbf{E}$ can be related as

$$\mathbf{J}(\mathbf{r}, t) = \int \int_{-\infty}^{t} \boldsymbol{\sigma}(\mathbf{r}, \mathbf{r}_1, t, t_1) \cdot \mathbf{E}(\mathbf{r}_1, t_1) dt_1 \, d\mathbf{r}_1, \tag{4}$$

where the volume integral is over the whole spatial domain of the plasma and the time integral accounts for electron trajectories at all previous times. For this expression to differ significantly from Ohm's law, there must also be significant spatial gradients in either the electric field or conductivity. In principle, Eq. (4) along with the appropriate $\boldsymbol{\sigma}$ can accurately describe plasma–electromagnetic wave interactions. The resultant equations are, however, complicated and they have only been solved analytically in a few simple situations. A well known example is that of a collisionless plasma in which spatial variations only occur in one direction. Analysis reveals the existence of an anomalous skin effect in such a situation. This effect has been studied in solid state as well as gaseous plasmas.[20,21]

Unfortunately, the numerical evaluation of Eq. (4) in multidimensional models is computationally expensive. The definition of an effective conductivity also entails approximations which limit the range of validity of the resulting model. If the goal of the simulation is to compute quasi-steady state plasma parameters, as opposed to startup or shutdown transients, a hybrid code that separates electron kinetics from the calculation of the electromagnetic field can be applied in an iterative manner to accurately address warm-electron and noncollisional heating effects. We have developed such an algorithm. We will first describe the hybrid model in which we have included noncollisional heating algorithms, and then discuss the algorithm.

The hybrid model in which we implemented noncollisional algorithms was previously described in detail, and so will be briefly described here.[13,22,23] The two-dimensional simulation, called the hybrid plasma equipment model (HPEM), consists of three coupled modules. In the electromagnetic module (EMM), Maxwell's equations are solved to obtain the electromagnetic fields that are generated by the external antenna and plasma currents. These electromagnetic fields are then used in the electron Monte Carlo simulation (EMCS) to determine the electron energy distribution function, transport coefficients, and electron impact source functions. Using these transport coefficients and source functions, particle densities and fluxes are computed in the fluid kinet-

ics simulation (FKS). Poisson's equation is also solved in FKS to obtain electrostatic fields. The electrostatic fields and species densities are cycled back to the EMCS, and the plasma conductivity is cycled back to the EMM. The procedure of iterating through the modules is repeated until the solution converges. Due to the symmetry of the reactor in the examples we will discuss, the antenna generated electric field and current have only azimuthal components.

The HPEM previously described used the cold-electron approximation in EMM, and Eqs. (1) and (2) were used to solve for the wave electromagnetic fields. Ion current was neglected since it is smaller than the electron current. Due to the fact that kinetic effects, including noncollisional heating, are by default included in the EMCS but not communicated back to the EMM this implementation will be referred to as the quasicollisional model. To fully account for noncollisional coupling back to the EMM in the HPEM, we include the following algorithms. In the EMCS, we follow electron trajectories in the temporally and spatially varying electric and magnetic fields produced by the EMM and FKS. This calculation is fully kinetic and makes no assumptions about the mechanism of electron transport. The resulting electron velocity distribution, $f_v(\mathbf{r},\phi)$ (ϕ is the phase in the rf cycle), therefore reflects all pertinent heating and cooling mechanisms. Using results from both the EMCS and FKS, we construct the kinetic azimuthal current density

$$\begin{aligned}\mathbf{J}_e(\mathbf{r}) &= J_0(\mathbf{r})\exp[i\phi_v(\mathbf{r})]\hat{\theta}\\ &= -qn_e(\mathbf{r})v_\theta(\mathbf{r})\exp[i\phi_v(\mathbf{r})]\hat{\theta}.\end{aligned} \tag{5}$$

In Eq. (5) $n_e(\mathbf{r})$ is the electron density determined by the FKS, $v_\theta(\mathbf{r})$ is the amplitude of the azimuthal electron velocity at the fundamental frequency, and $\phi_v(\mathbf{r})$ is the relative phase of the local electron velocity. The azimuthal electron velocity $\mathbf{v}_e(\mathbf{r})=v_\theta(\mathbf{r})\exp[i\phi_v(\mathbf{r})]$ is obtained by sampling the electron pseudoparticles during the EMCS, binning them according to speed, location, and phases, and performing a discrete Fourier transform to isolate the component at the fundamental harmonic. $\mathbf{J}_e$ is then cycled back to the EMM, and the modules are iterated in the usual fashion. The additional calculation of $\mathbf{J}_e$ adds negligible computer time to the simulation.

For computational purposes, we divided $\mathbf{J}_e$ which is cycled back to the EMM into two components,

$$\mathbf{J}_e=\sigma\mathbf{E}+\mathbf{J}_{\text{res}}, \tag{6}$$

where σ is given by Eq. (2) and $\mathbf{J}_{\text{res}}$ is the density of residual current produced due to warm-electron effects. The purpose of couching $\mathbf{J}_e$ in this manner is to provide computational stability in the solution of Maxwell's equation, which in our case uses the method of successive overrelaxation (SOR). For parameter regimes where the cold-electron approximation is valid, $|\mathbf{J}_{\text{res}}|\ll|\mathbf{J}_e|$, and the results from this self-consistent model and a model that only considers collisional heating should be similar. However, when warm-electron effects come into play, the characteristics of the plasma are modified.

It should be noted that in the previously described HPEM, which used $\mathbf{J}_e=\sigma\mathbf{E}$ in the EMM, noncollisional heating of electrons is indeed captured in the EMCS module and so is included in the calculation of electron impact rate and transport coefficients. The EMCS captures all pertinent heating mechanisms for the given electric fields. The improvements we discuss here pertain to the self-consistent coupling of those heating mechanisms with the electromagnetic calculation. The power deposition obtained from the EMCS, which includes noncollisional effects, is defined as the kinetic power deposition, P_k. This time average power deposition is calculated from

$$P_k=\frac{1}{\tau}\int_0^\tau\int qn_e(\mathbf{r})v_e(\mathbf{r},t)\mathbf{E}(\mathbf{r},t)d^3r\ dt, \tag{7}$$

where $n_e(\mathbf{r})$is obtained from the FKS and $v_e(\mathbf{r})$ is obtained by sampling the electron trajectories over the rf period τ.

It is not possible to completely isolate noncollisional electron heating from collisional heating in the EMCS since it is a kinetic calculation. Therefore to make comparisons between fully collisional and noncollisional representations, we replaced the EMCS with the Boltzmann electron energy equation module (BEM). In doing so, all electron transport is collisional. In the BEM we solve an electron energy equation for average energy ϵ,[23]

$$\frac{\partial(n_e\epsilon)}{\partial t}=P(\epsilon)-n_e\sum_i N_i\kappa_i-\nabla\left(\frac{5}{2}\epsilon\varphi-\lambda\nabla T_e\right), \tag{8}$$

where $T_e\equiv(2\epsilon/3)$ is the electron temperature, n_e is the electron density (obtained from the FKS), P is the electron power deposition (obtained from the EMM and FKS), κ_i is the rate coefficient for power loss (eV cm^3 s^{-1}) for collisions of electrons with species i having density N_i (the latter obtained from the FKS), λ is the electron thermal conductivity, and φ is the electron flux (obtained from the FKS). This equation is solved in the steady state using an implicit SOR technique. An electron temperature of 0.05 eV is assigned to all surfaces in contact with the plasma and the thermal conductivity is assigned appropriately small values across the sheath commensurate with the electron density in the sheath. This effectively results in an adiabatic boundary condition.

The electron transport coefficients and rate coefficients used in solving Eq. (8) are obtained by solving Boltzmann's equation (BE) using a two-term spherical harmonic expansion.[24] BE is parameterized over a range of E/N, and a table of transport coefficients as a function of ϵ is constructed. This table is then interpolated during solution of Eq. (8). The electron energy equation and BE (to generate the lookup table) are solved on each iteration through the simulation based on updated densities, mole fractions, fluxes, and power deposition.

III. NONCOLLISIONAL HEATING IN ICP REACTORS

We will now discuss results from simulations of ICP reactors which include noncollisional electron heating in the plasma–electromagnetic (EM) wave interaction. The extent to which warm-electron noncollisional heating effects come into play depends on gas pressure, input power, gas mixture, and geometry in a complicated manner. One can, however, draw the general conclusion that, when only collisional

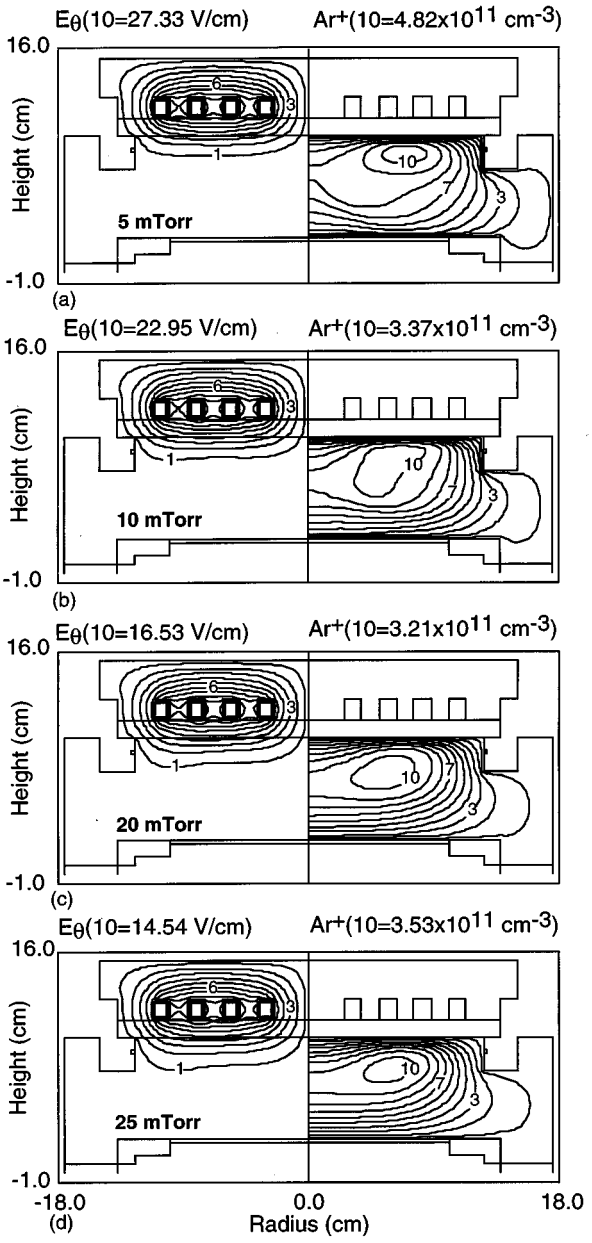

FIG. 1. Azimuthal electric field amplitude and Ar^+ density from the quasicollisional model for gas pressures of (a) 5, (b) 10, (c) 20, and (d) 25 mTorr. The power deposition is 600 W in argon.

power transfer mechanisms are considered in coupling plasma dynamics to the EM wave, specific power deposition (watts/electron) is lower than when noncollisional mechanisms are also employed. As a consequence, for constant total power deposition, a self-consistent model that includes both collisional and noncollisional mechanisms predicts lower plasma densities than a model that only considers collisional heating. The self-consistent model also predicts that electromagnetic waves will penetrate deeper into the plasma.

The geometry we used in our study is shown in Fig. 1. The ICP reactor is powered by a four-turn spiral coil set on top of a 1.5-cm-thick quartz window. The coil is driven at 13.56 MHz. The window to substrate separation is 7.5 cm. The substrate holds a 20-cm-diam silicon wafer surrounded by an alumina focus ring. The reactor is described in more detail in Refs. 13 and 22. For the cases discussed here, we apply power only to the coil; no substrate bias is used. We investigated Ar, O_2, N_2, and Ar/Cl_2 plasmas. These reaction chemistries are discussed in Ref. 13. For the O_2 and Ar/O_2 cases, we also added electron impact momentum transfer, excitation, and ionization of atomic oxygen to the reaction set. The cross sections for these processes were obtained from Ref. 25. Continuity and momentum conservation equations were solved for all heavy particle species.[22]

The plasma density and electric field amplitude for pressures of 5, 10, 20, and 25 mTorr are shown in Fig. 1 for an Ar plasma using a quasicollisional model where we consider only collisional heating in the EMM. The plasma density and electric field amplitude are shown in Fig. 2 using the noncollisional model in which electron dynamics are self-consistently coupled to the electromagnetic field computation. The total inductively coupled input power, defined as $\int J \cdot E d^3 r$, was kept constant at 600 W. In the quasicollisional model, Eq. (2) is used for the electron current density in the solution of Maxwell's equations, whereas the EMCS is used for electron transport. The power deposition computed in the EMM is therefore a lower limit to the power which is kinetically transferred to the electrons in the EMCS. The total power deposition into the electrons which is captured by the EMCS unavoidably contains noncollisional effects, even when the electromagnetic-plasma coupling in the EMM is collisional, and so will be larger. As noted above, to distinguish these conditions from a fully collisional situation, we refer to this coupling as quasicollisional.

The electric field amplitude and plasma density profiles predicted by the noncollisional and collisional models are similar at 25 mTorr. At this pressure, $\nu_m \sim \omega$, and the electron dynamics in the EMM can adequately be described using the cold-electron approximation. The electron transport in the EMCS is also sufficiently collisional that the local kinetically derived power deposition is essentially given by σE^2. As the pressure is decreased, the quasicollisional and self-consistent noncollisional formulations begin to diverge. In the self-consistent case, warm-electron and long mean free path effects cause the electromagnetic wave to couple more efficiently to the plasma. Lower electric fields and plasma densities are, therefore, required to deposit the same total power. In the quasicollisional case, the reduction in the efficiency of coupling predicted by Eq. (2) in the EMM requires a larger plasma density to produce the same power deposition, and so the electron density increases. While the shape of the profiles do not seem to be significantly modified, the peak plasma density predicted by the self-consistent model is a factor of 3.7 smaller at 5 mTorr as compared to the quasicollisional cold-electron model. One can also observe that the electric field penetrates deeper into the plasma when warm-electrons effects are included which may be attributed in part to the lower plasma density. There are two effects that contribute to these results. First, the EM coupling in the fully noncollisional model is more efficient. Therefore, at constant power deposition, the plasma density is lower. Second, the kinetic power deposition derived in the EMCS, which ultimately determines the ionization rates, is increasingly larger than the collisional power used in the EMM as the pressure

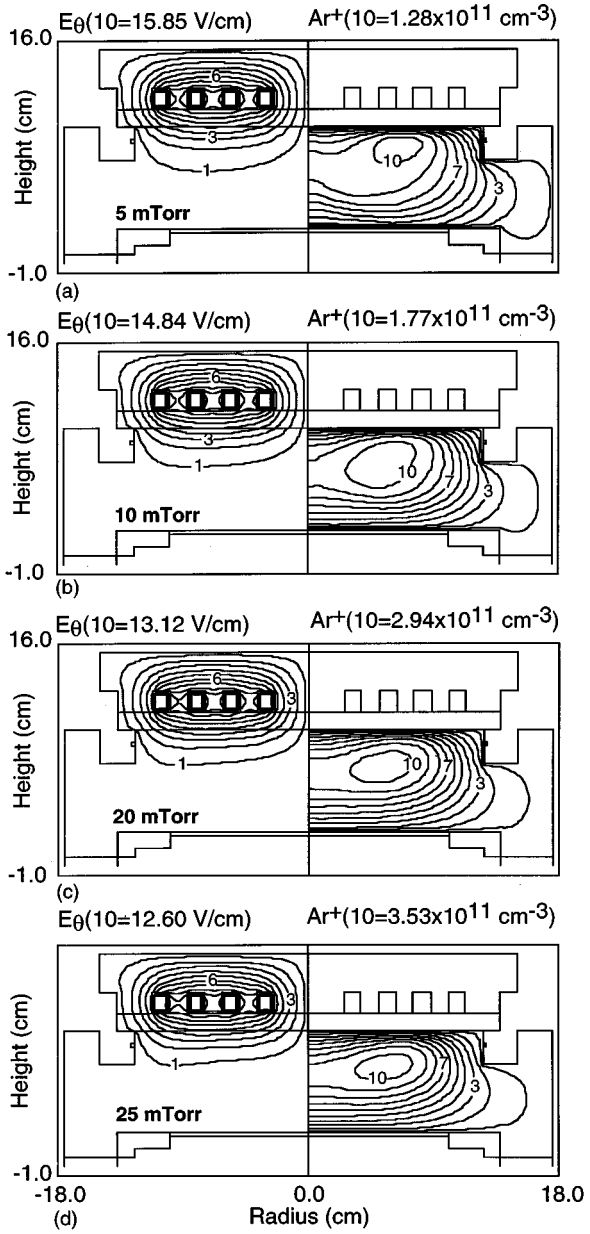

FIG. 2. Azimuthal electric field amplitude and Ar^+ density from the noncollisional model for gas pressures of (a) 5, (b) 10, (c) 20, and (d) 25 mTorr. The conditions are the same as for Fig. 1. Although the plasma density profiles are similar to the quasicollisional model, the peak plasma densities are lower when using the noncollisional model due to the disparity between purely collisional and kinetic power deposition.

is decreased as shown in Fig. 3. This leads to a larger plasma density.

The impact of noncollisional heating in the dynamics of low pressure ICPs is illustrated in Fig. 4 where we have plotted the peak Ar^+ density (equal to the electron density for those conditions) as a function of pressure for different models of EM coupling. The power deposition as calculated in the EMM is kept constant at 600 W. Since the plasma profile does not change significantly in the pressure range of 5–25 mTorr, the average plasma densities will have similar results. The Ar^+ density as a function of pressure has been measured in a variety of ICP reactors by several researchers including Godyak *et al.*,[9] Keller *et al.*,[25] Hopwood *et al.*,[6]

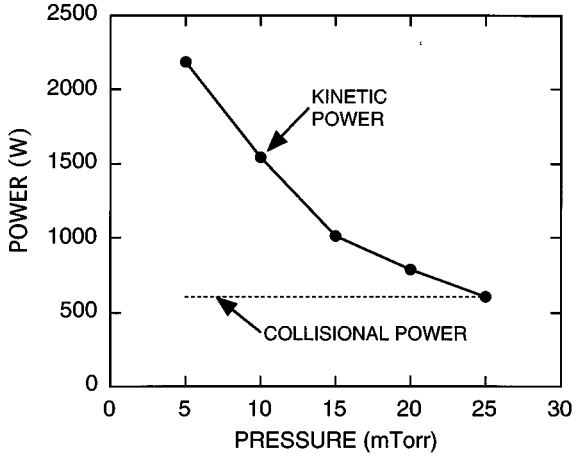

FIG. 3. Kinetic power deposition for a constant collisional power deposition for the conditions of Fig. 1.

and Mahoney *et al.*[3] All their results show that Ar^+ density decreases as pressure is decreased. The fully noncollisional model predicts that the electron density decreases with decreasing pressure. The quasicollisional model predicts plasma densities increase with decreasing gas pressure. This trend results from the increasing disparity between the collisional power deposition predicted by the cold-electron approximation in the EMM and kinetic power deposition captured in the EMCS as the pressure decreases (see Fig. 3). The plasma density predicted by the fully collisional model also decreases with decreasing pressure, although not to the degree of the noncollisional model. (It should be noted that the spatial distribution of plasma density is different in the fully collisional case.) This trend results from the decreasing coupling efficiency which reduces σ (for a given plasma density) as the pressure decreases and ω/ν_m increases. A larger plasma density is required to recoup this loss. The fact that

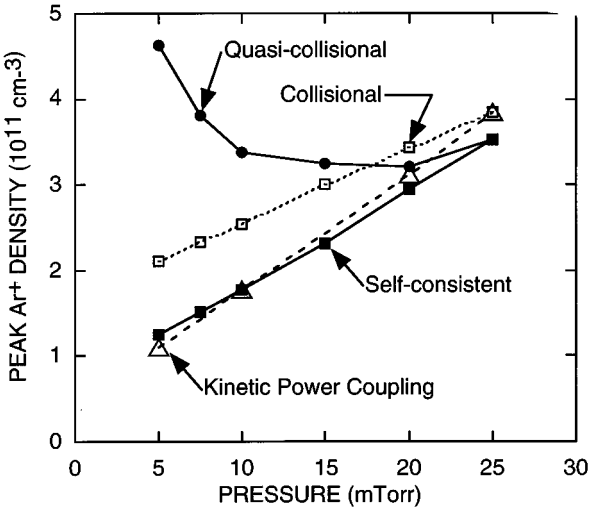

FIG. 4. Peak plasma density as a function of pressure for a power deposition of 600 W in an argon plasma. Results are shown for quasicollisional, noncollisional, and collisional models. As the pressure is decreased below 20 mTorr, the disparity between the results of the quasicollisional and collisional models with those from the collisional models increases.

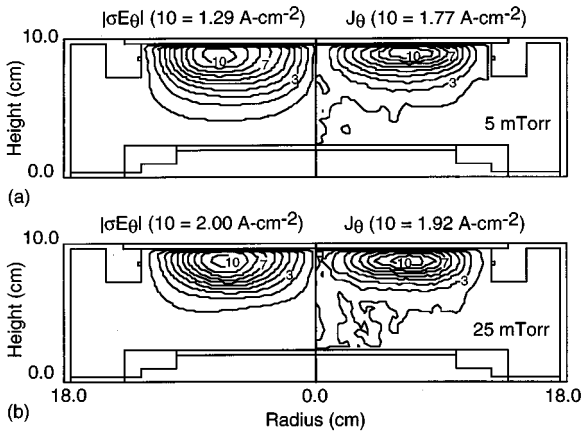

FIG. 5. Comparison of the collisional current density $E_\theta\sigma$ with the kinetically derived current density J_θ at 5 and 25 mTorr in Ar. The electric field amplitude is the same for $E_\theta\sigma$ and J_θ at each pressure. At 25 mTorr $E_\theta\sigma$ and J_θ are essentially the same. At 5 mTorr, the noncollisional current is larger.

the ion density in the fully collisional model decreases with decreasing pressure is, to some degree, fortuitous since the collisional power deposition differs to such a degree from the kinetic power deposition. This is not a general result, as is discussed below.

Another measure of the efficiency of collisional versus noncollisional transport is shown in Fig. 5, where we have compared the collisional current density (σE_θ) with the kinetically derived current density (J_θ) for the same plasma conditions. At 25 mTorr, the peak magnitudes of σE_θ and J are essentially the same. At 5 mTorr, J_θ exceeds σE_θ by about 35% for the same electric field amplitude.

Regardless of the method, self-consistent coupling of the plasma dynamics with the EM field computation is, as a minimum, required to obtain the correct trend of Ar^+ density as a function of pressure. By self-consistent, we mean that the same heating mechanisms are employed in the simulation of the plasma as in the EM calculation. In the results shown in Fig. 4, the noncollisional and fully collisional cases capture the proper trends, even though the physics in the collisional case is known to be inaccurate. The quasicollisional case which uses the cold-electron approximation in the EM and noncollisional kinetics in the EMCS does not necessarily properly represent experimental trends. These results are, in part, a consequence of the fact that as long as all methods are conservative, the correct trends are in general captured. For example, fluid simulations for rf capacitively coupled discharges generate nearly the same plasma properties as kinetic particle-in-cell (PIC) simulations over a wide range of pressures.[26] Gas flow through plasma processing reactors having large Knudsen numbers modeled using the Navier–Stokes equations produce essentially the same results as direct simulation Monte Carlo (DSMC) simulations.[27]

The fortuitous agreement between fully collisional and noncollisional simulations requires that some conservative quantity be held constant, in this case total power deposition. By choosing power deposition as a normalizing factor, the electric fields in the collisional and noncollisional cases may be different while the same plasma density is obtained.[28] If, however, the quantity being held constant is coil current (an ''external'' parameter), the electric field would be fixed. Different ''self-consistent'' approaches would then generate different solutions.

When electrons are cold (i.e., only collisional heating is important), they are only affected by the electric field at their own location. As the electron temperature is increased and mean free path is increased, the random component of motion becomes commensurately larger. The electron velocity at a particular location and time is, therefore, not only dependent on the instantaneous local conditions but also on the conditions along their trajectories at past times. This nonlocal effect is the source of differences one observes between the predictions of warm- and cold-electron plasma models. It can be expected that these differences will become more pronounced as the electron Knudsen number ($\mathrm{Kn}_e=\lambda_e/L$; λ_e=electron mean free path, L=characteristic length) increases. This is precisely what happens when pressure is decreased. At lower pressures, the electron mean free paths are longer. The electrons, therefore, experience electric fields over larger extents of the plasma between collisions and the differences between the cold- and warm-electron models are greater. The same reasoning can be used to predict that warm-electron effects will have a greater impact at higher powers. At higher power deposition, the skin depth for electromagnetic field penetration is shorter. The electron Knudsen number Kn_e based on the region of high electric field is, therefore, larger. Electrons scatter in and out of the high electric field region more frequently, and warm-electron effects are therefore more pronounced. This argument is corroborated by our simulation results. As an example, we show simulation results for power deposition of 100 and 1200 W in Fig. 6 for the fully collisional and quasicollisional cases. The pressure is 5 mTorr and the simulations were performed in Ar. Note that at the higher power deposition and plasma density the skin depth and penetration of the electric field into the plasma are shorter. This results in more severe gradients in the electric field at the higher power deposition compared to the collisional case, which should emphasize noncollisional effects to a greater degree. This trend is shown by the results of the simulations. At lower power, the case for quasicollisional power deposition overpredicts the plasma density by a factor of 2.4, whereas at the higher power deposition, where noncollisional effects should be more prevalent, the quasicollision case overpredicts plasma density by a factor of 3.4.

We found that the majority of the effects of noncollisional heating can be captured using the quasicollisional model provided that the resulting electric fields are normalized by the kinetic power deposition. The procedure we followed is as follows. In the EMCS, we calculate the kinetic power deposition using Eq. (7). Assuming a collisional model for Eq. (1), the collisional power deposition is the calculation from Eq. (3). The electric field amplitude which is next used in the EMCS is normalized by

$$E_0 \rightarrow E_0 \left(\frac{P_c}{P_k} \right)^{1/2}. \tag{9}$$

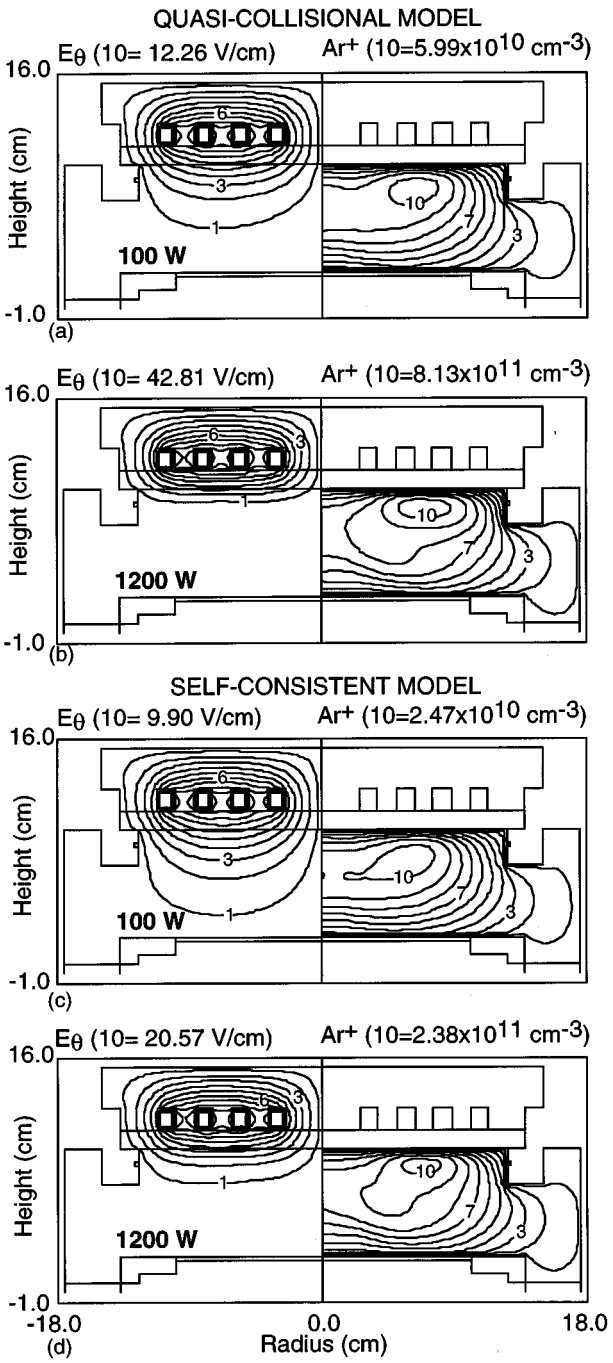

FIG. 6. Azimuthal electric field amplitude and Ar^+ density at 5 mTorr of Ar at powers of 100 and 1200 W from the quasicollisional heating model (a) and (b); and the noncollisional model (c) and (d).

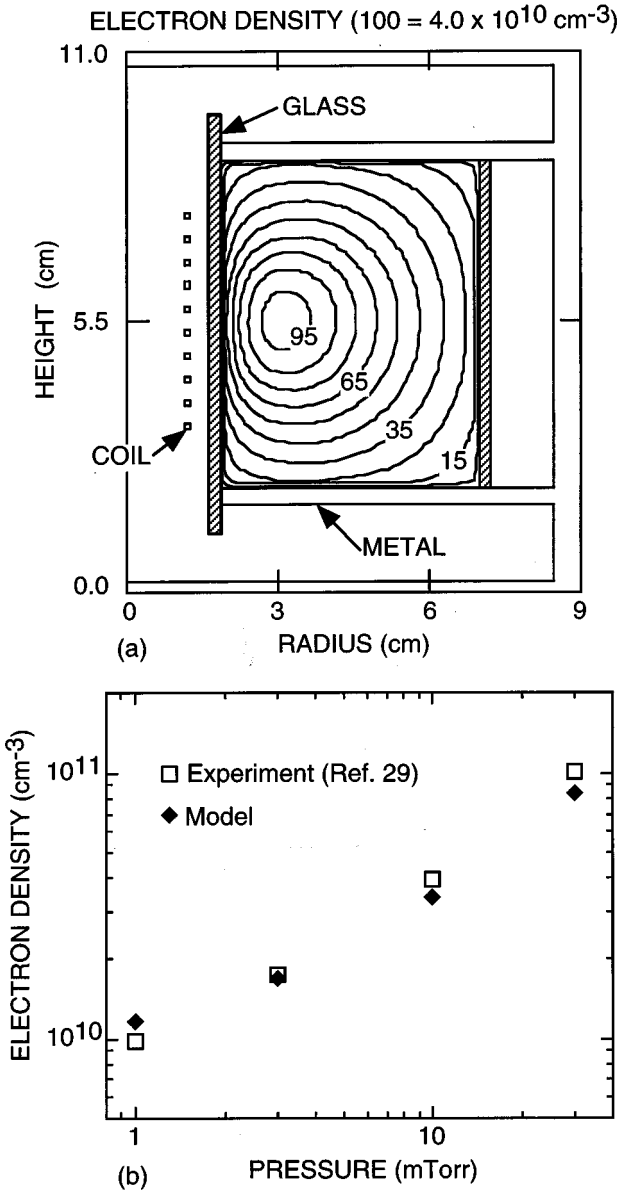

FIG. 7. Computed electron densities at 50 W power deposition for the experimental conditions of Ref. 29. (a) Electron density as a function of position; (b) plasma density 0.5 cm from the inner wall. The computational results, obtained using noncollisional power normalization, quantitatively capture the experimental results.

Using this algorithm, the peak plasma densities as a function of pressure in Ar plasmas are shown in Fig. 3. The plasma densities decrease with decreasing pressure as in the fully noncollisional model, and nearly reproduce the results obtained with the fully noncollisional model.

To further confirm the appropriateness of the power normalization scheme in correcting noncollisional heating effects in the EMM, we validated the method by comparing results from the model to experiments conducted by Godyak, Piejak, and Alexandrovich.[29] The experimental discharge chamber uses an ''internal'' ten-turn coil surrounded by a Faraday shield to minimize capacitive coupling. The plasma region is between two coaxial glass cylinders with 3.8 and 14.2 cm internal diameters, mounted between aluminum plates separated by 6.7 cm. For the results discussed here, the discharge power deposition is held constant at 50 W and the gas pressure is varied. The computed electron density at 10 mTorr and a comparison of computed electron density to experimental values as a function of pressure are shown in Fig. 7. The power normalization method quantitatively captures the experimental trend of decreasing electron density with decreasing pressure for a constant power deposition.

We also compared results from the self-consistent fully collisional model for pure O_2, N_2, and $Ar/Cl_2=70/30$ plasmas with results obtained from the self-consistent noncollisional model. [To obtain the noncollisional results, we have

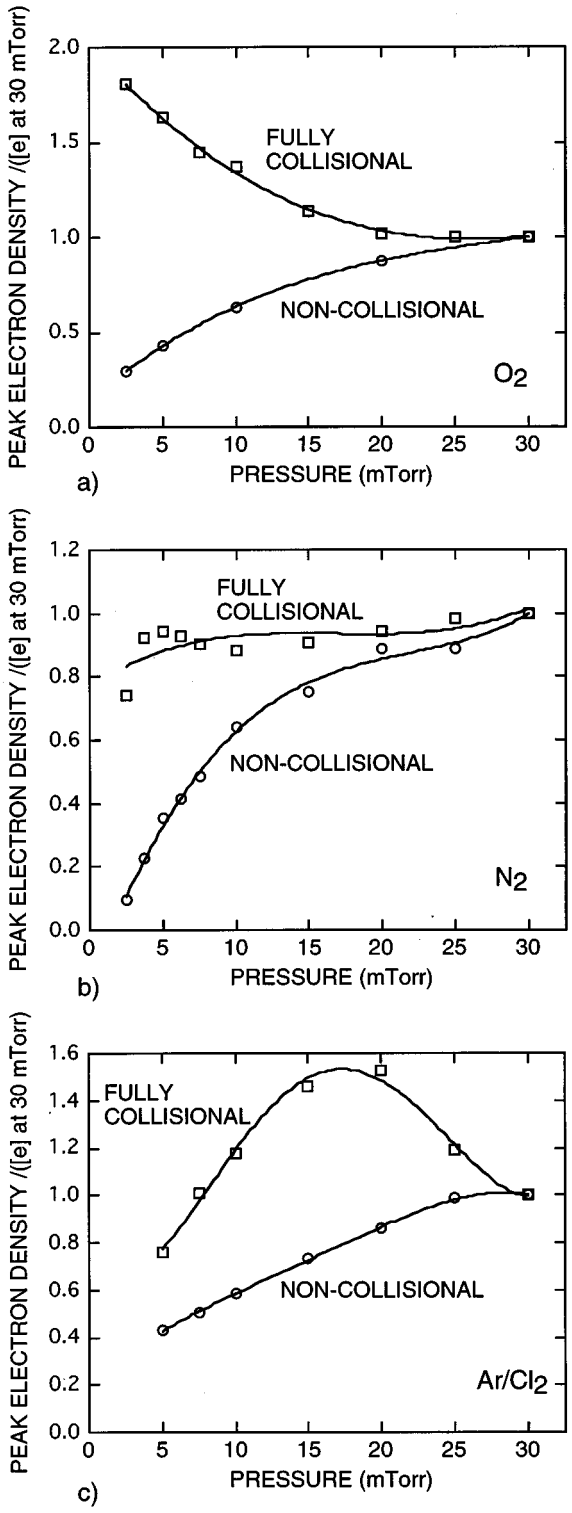

FIG. 8. Peak electron densities in (a) O_2, (b) N_2, and (c) Ar/Cl_2=70/30 gas mixtures for 600 W power deposition as a function of pressure. Results are shown for fully collisional and noncollisional algorithms using power normalization.

renormalized the electric fields using the kinetically derived power deposition as described by Eq. (9).] The maximum electron density as a function of gas pressure is shown in Fig. 8 for power depositions of 600 W. For purposes of comparison, we normalized the electron density to its value at 30 mTorr. In all cases, the electron density obtained with the noncollisional model decreases with decreasing pressure. The electron density obtained with the fully collisional model increases for O_2, is relatively constant for N_2, and has a maximum at an intermediate pressure for Ar/Cl_2. It is difficult to extract trends from these results which can be applied elsewhere. One can, however, conclude that the details of comparison between collisional and noncollisional algorithms strongly depend on the details of the momentum transfer and energy loss cross sections. Collisional and noncollisional algorithms which generate the same plasma properties in the pressure regimes of interest may be a fortuitous consequence of the chosen set of cross sections.

The antenna used in previous simulations produced electric fields that had an almost flat profile in the radial direction and decayed exponentially in the axial direction. Noncollisional heating, therefore, occurred primarily during the axial motion of the electrons. If the fields are inhomogeneous in more than one direction, electrons can be noncollisionally heated while they move in other directions as well. For example, we produced an inhomogeneous electric field by using a single-turn antenna for the geometry in Fig. 1. As a result, the electric field expands in both axial and radial directions thereby noncollisionally heating electrons during their radial motion as well as during their axial motion as for the four-turn antenna. We compared results for the single-turn antenna in Ar at 5 mTorr (600 W) for the noncollisional and quasicollisional models. The electric field required to sustain the plasma using the noncollisional model is 0.52 that of the quasicollisional model for the one-turn antenna. With the four-turn coil, which produces dominant noncollisional heating only in the axial direction, the electric field in the noncollisional model is 0.77 that of the quasicollisional model. The lower electric field required with the one-turn antenna reflects the additional noncollisional heating obtained in the radially inhomogeneous electric fields.

IV. CONCLUSIONS

In this article, we described an algorithm to self-consistently incorporate warm-electron effects and noncollisional heating in inductively coupled plasma models. The algorithm is simple to implement, requires little extra computational time, and is general enough to be used with any plasma chemistry and geometry. The method involves computing the current density due to the azimuthal electric field using a kinetic scheme, in this case a Monte Carlo simulation, and using the current to correct the collisional current density used in solution of Maxwell's equations. We found that, when including noncollisional heating in a self-consistent manner at pressures below 10–20 mTorr, the electromagnetic wave coupling is more efficient. Therefore, for a given power deposition, the plasma density can be lower than that obtained with a fully collisional model. The trends observed with the self-consistent noncollisional model can be captured by a simulation using a collisional current in the electromagnetics calculation if the fields are normalized by the kinetically derived power. We also found that self-consistent, fully collisional models can, in some cases, capture the appropriate systematic behavior at low pressures as

was obtained in self-consistent collisional models provided the specified parameter such as power deposition, as opposed to coil current, is conservative. This finding is, however, sensitive to the working gas. Noncollisional and fully collisional models had moderately good agreement for plasma density as a function of pressure for Ar but had poor agreement for N_2, O_2, and Ar/Cl_2.

[1] D. K. Coultas and J. H. Keller, European Patent No. 0 379 828 A2 (1990).
[2] J. S. Ogle, U.S. Patent No. 4,948,458 (1990).
[3] L. J. Mahoney, A. E. Wendt, E. Barrios, C. J. Richards, and J. L. Shohet, J. Appl. Phys. **76**, 2041 (1994).
[4] V. I. Kolobov, D. F. Beale, L. J. Mahoney, and A. E. Wendt, Appl. Phys. Lett. **65**, 537 (1994).
[5] J. Hopwood, C. R. Guarnieri, S. J. Whitehair, and J. J. Cuomo, J. Vac. Sci. Technol. A **11**, 147 (1993).
[6] J. Hopwood, C. R. Guarnieri, S. J. Whitehair, and J. J. Cuomo, J. Vac. Sci. Technol. A **11**, 152 (1993).
[7] J. Hopwood, Appl. Phys. Lett. **62**, 940 (1993).
[8] J. Hopwood, Plasma Sources Sci. Technol. **3**, 460 (1994).
[9] V. A. Godyak, R. B. Piejak, and B. M. Alexandrovich, Plasma Sources Sci. Technol. **4**, 332 (1995).
[10] R. Piejak, V. Godyak, and B. Alexandrovich, J. Appl. Phys. **78**, 5296 (1995).
[11] P. A. Miller, G. A. Hebner, K. E. Greenberg, P. A. Pochan, and B. P. Aragon, J. Res. Natl. Inst. Stand. Technol. **100**, 427 (1995).
[12] G. A. Hebner, J. Appl. Phys. **80**, 2624 (1996).
[13] P. L. G. Ventzek, R. J. Hoekstra, and M. J. Kushner, J. Vac. Sci. Technol. B **12**, 461 (1994).
[14] G. DiPeso, V. Vahedi, D. W. Hewett, and T. D. Rognlien, J. Vac. Sci. Technol. A **12**, 1387 (1994).
[15] R. A. Stewart, P. Vitello, D. B. Graves, E. F. Jaeger, and L. A. Berry, Plasma Sources Sci. Technol. **4**, 36 (1995).
[16] D. P. Lymberopoulos and D. J. Economou, J. Vac. Sci. Technol. A **12**, 1229 (1994).
[17] M. M. Turner, Phys. Rev. Lett. **71**, 1844 (1993).
[18] V. A. Godyak, R. B. Piejak, and B. M. Alexandrovich, Plasma Sources Sci. Technol. **3**, 169 (1994).
[19] V. Vahedi, M. A. Lieberman, G. DiPeso, T. D. Rognlien, and D. Hewett, J. Appl. Phys. **78**, 1446 (1995).
[20] S. Ichimaru, *Basic Principles of Plasma Physics: A Statistical Approach* (Benjamin, Reading, MA, 1973), p. 84.
[21] A. B. Pippard, Proc. R. Soc. London, Ser. A **191**, 385 (1947).
[22] W. Z. Collison and M. J. Kushner, Appl. Phys. Lett. **68**, 903 (1996).
[23] M. J. Kushner, W. Z. Collison, M. J. Grapperhaus, J. P. Holland, and M. S. Barnes, J. Appl. Phys. **80**, 1337 (1996).
[24] See, for example, W. L. Morgan and B. M. Penetrante, Comput. Phys. Commun. **58**, 127 (1990).
[25] Y. Itikawa and A. Ichimura, J. Phys. Chem. Ref. Data **19**, 637 (1990).
[26] T. E. Nitschke and D. B. Graves, J. Appl. Phys. **76**, 5646 (1994).
[27] V. Singh, B. Berney, and A. Krishnan, J. Vac. Sci. Technol. A **14**, 1252 (1996).
[28] M. Turner has expressed a similar conclusion in private communications based on work in Ref. 17 and subsequent studies.
[29] V. A. Godyak, R. B. Piejak, and B. M. Alexandrovich, Plasma Sources Sci. Technol. **4**, 332 (1995).